American Mineralogist, Volume 66, pages 278–289, 1981

Carbonates and pyroxenoids from the manganese deposit near Bald Knob, North Carolina[1]

GARY A. WINTER,[2] ERIC J. ESSENE AND DONALD R. PEACOR

Department of Geological Sciences, University of Michigan
Ann Arbor, Michigan 48109

Abstract

Studies of minerals from a metamorphosed manganese deposit at Bald Knob, North Carolina, yield estimates of temperatures and local fluid compositions at the peak of metamorphism. Electron microprobe analyses of Mn–Ca carbonates demonstrate that they span the rhodochrosite–kutnahorite solvus without a break, suggesting metamorphic temperature >550°C. The adjacent mid-amphibolite facies metamorphism implies temperatures not greatly exceeding this value. Pressure is estimated at 5±1 kbar based on nearby occurrences of aluminosilicates. Compositional data on coexisting rhodonite and pyroxmangite suggests that a narrow miscibility gap separates the two phases at these P–T conditions. The assemblage rhodonite/pyroxmangite–rhodochrosite–quartz requires water-rich fluids during metamorphism. The common occurrences of the accessory minerals cattierite (CoS_2), alabandite (MnS), and pyrophanite ($MnTiO_3$) at Bald Knob require a relatively reduced and sulfidizing local metamorphic environment. Occasional finds of rhodonite/pyroxmangite–alabandite–quartz and rhodonite/pyroxmangite–tephroite–alabandite restrict fO_2/fS_2 to a narrow band between $10^{-19}/10^{-3}$ and $10^{-16}/10^{0}$. Conditions were probably buffered throughout metamorphism by reaction of a sulfur-rich, oxygen-poor protolith.

Introduction

The manganese deposit near Bald Knob, North Carolina, is located in Alleghany County, in the northwest region of the state. Sparta, North Carolina, lies about 3 miles southwest, and Bald Knob is a half mile northwest. The deposit is enclosed by Precambrian–early Paleozoic amphibolites, mica schists, and garnet–mica schists of the Piedmont terrane.

The deposit was first described by Ross and Kerr (1932) who reported two new minerals, galaxite and alleghanyite. More recently, Peacor *et al.* (1974) described another new mineral, kellyite, from this deposit. The idealized formulae of these minerals and those mentioned below are given in Table 1, along with their structure types. Although Ross and Kerr ascribed a hypogene vein origin for the manganese-rich body, the deposit probably represents an original sediment composed primarily of quartz, manganese carbonates, sulfides, and oxides, which was subsequently metamorphosed to yield the present assemblages. This conclusion is supported by data showing that the temperature for the deposit is compatible with that inferred from the local metamorphic assemblages.

Two parageneses, carbonate-rich and quartz-rich, exist at Bald Knob. The carbonate-rich rocks are now undersaturated in SiO_2 and consist primarily of Mn–Ca carbonates, alleghanyite, sonolite, manganhumite, tephroite, galaxite, jacobsite, and kellyite, with accessory alabandite, cattierite, cobaltite, apatite, caryopilite, and pyrophanite. The quartz-rich rocks contain quartz, spessartine, rhodonite, pyroxmangite, Mn–Ca carbonate, tirodite, with minor pyrophanite and galaxite. The rocks are banded, and the constituent grains show typical interlocking metamorphic textures. The banding results from concentrations of one or more of the phases, probably reflecting original sedimentary variations. These observations lend support for a metamorphic origin of the deposit, as opposed to the vein origin suggested

[1]Contribution No. 362 from the Mineralogical Laboratory, Department of Geological Sciences, University of Michigan, Ann Arbor, Michigan 48109.

[2]Present address: Tennessee Valley Authority, P.O. Box 2957, Casper, Wyoming 82602.

0003–004X/81/0304–0278$02.00

Table 1. Unusual Bald Knob minerals, their ideal formulae and structure types

Mineral	Formula	Structure
pyrophanite	$MnTiO_3$	ilmenite
galaxite	$MnAl_2O_4$	spinel
jacobsite	$MnFe_2O_4$	spinel
alabandite	MnS	halite
cattierite	CoS_2	pyrite
cobaltite	CoAsS	arsenopyrite
alleghanyite	$(Mn_2SiO_4)_2Mn(OH,F)_2$	chondrodite
manganhumite	$(Mn_2SiO_4)_3Mn(OH,F)_2$	humite
sonolite	$(Mn_2SiO_4)_4Mn(OH,F)_2$	clinohumite
tephroite	Mn_2SiO_4	olivine
spessartine	$Mn_3Al_2Si_3O_{12}$	garnet
rhodonite	$MnSiO_3$	rhodonite
pyroxmangite	$MnSiO_3$	pyroxmangite
kutnahorite	$CaMn(CO_3)_2$	dolomite
tirodite	$Mn_2Mg_5Si_8O_{22}(OH)_2$	tremolite
kellyite	$Mn_4Al_4Si_2O_{10}(OH)_2$	serpentine
caryopilite	$Mn_8Si_6O_{15}(OH)_{10}$*	friedelite

*Peacor and Essene (1980)

by Ross and Kerr. Our discussion is predicated on the assumption that the Bald Knob deposit was indeed equilibrated during the peak of regional metamorphism. The experimental and thermodynamic data on manganese carbonate, silicate, and sulfide systems are applied to determine the metamorphic conditions at which the Bald Knob assemblages formed.

Carbonate thermometry

Quantitative electron microprobe analyses of carbonate minerals from the Bald Knob deposit suggest that they can be approximated by the ternary system $CaCO_3$–$MnCO_3$–$MgCO_3$. Goldsmith and Graf (1957) investigated subsolidus relations in the system $CaCO_3$–$MnCO_3$ and found a solvus in the Mn-rich half of the system. They found complete solid solution between calcite and rhodochrosite above 550°C. One limb of the solvus approaches a 1:1 Ca:Mn composition at about 450°C, indicating a high degree of cation ordering below this temperature corresponding to kutnahorite, $CaMn(CO_3)_2$. Goldsmith and Graf (1960) also investigated subsolidus relations in the ternary system $CaCO_3$–$MnCO_3$–$MgCO_3$ at various temperatures at a total pressure of 10 kbar. Their exploratory runs in the pressure range 2 to 15 kbar indicate that the effect of pressure on the relations is small, and in our study their results are assumed to be directly applicable to assemblages which equilibrated at ~5 kbar. The solvus in the Mn-rich part of the $CaCO_3$–$MnCO_3$ system widens slightly with increasing $MgCO_3$ as it extends into the ternary system. At 600°C there is complete solid solution of Ca–Mn–Mg carbonates in the Ca-poor half of the sytem for those compositions with less than 17 mole percent $MgCO_3$. These systems may be used to estimate the temperature at which natural Ca–Mn carbonates equilibrated. Carbonates from the Bald Knob deposit were analyzed and compared to the phase relations in order to restrict their temperature of equilibration.

Exploratory X-ray diffraction studies of many Bald Knob carbonates showed a wide range of Ca–Mn solid solution (Stein, written communication). Subsequent partial analyses by electron microprobe showed that Mn and Ca are the major cations in these carbonates, with Mg and Fe present in only minor amounts. Eleven thin sections with carbonate compositions that would span the general range of values found previously were chosen for more complete analysis. A total of 67 grains from these sections was analyzed on an ARL-EMX electron microprobe at The University of Michigan. Details of the analytical procedures are given in the appendix.

Discussion

After converting the carbonate analyses to mole percent and extracting the carbonate components, the carbonates range from Cc_7Rc_{93}[3] to $Cc_{73}Rc_{27}$ with less than 10% $(Mg,Fe)CO_3$. These compositions are plotted on a ternary diagram (Fig. 1), where $FeCO_3$ is combined with $MgCO_3$ because their effects on the solvus are approximately the same at low concentrations. Increasing the $MgCO_3$ component of Ca–Mn carbonates widens the solvus extending out from the $CaCO_3$–$MnCO_3$ binary and presumably raises its upper temperature limit to some extent. Bald Knob carbonate compositions are apparently uninterrupted by the solvi in the system, and we infer that the minimum temperature of equilibration of these carbonates was greater than 550°C, the peak of the kutnahorite–rhodochrosite solvus (Goldsmith and Graf, 1957). Country rocks are muscovite–oligoclase–

[3] Cc = calcite ($CaCO_3$), Rc = rhodochrosite ($MnCO_3$).

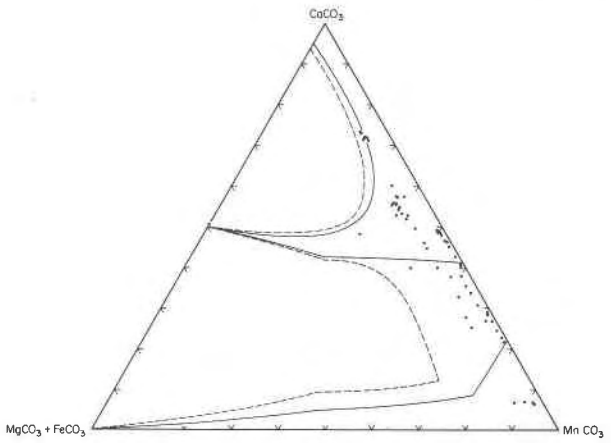

Fig. 1. Triangular composition diagram superimposed on the phase diagram of the $CaCO_3$–$MgCO_3$–$MnCO_3$ system, showing the solvi at 500°C (after Goldsmith and Graf, 1960). Bald Knob carbonate compositions are plotted. $FeCO_3$ is combined with $MgCO_3$ in this plot. Dashed boundaries show the position of the solvi at 600°C.

quartz–garnet–mica schists and hornblende–andesine±cummingtonite±magnetite amphibolites, representing medium-grade amphibolite facies metamorphism. These assemblages suggest maximum temperatures of about 550°–600°C during the metamorphism. The temperature during the metamorphism of the Bald Knob deposit is estimated at 575±40°C.

Frondel and Bauer (1955) described kutnahorite, $CaMn(CO_3)_2$, the manganese analogue of dolomite, from three localities. Carbonate analyses (Table 2) show that carbonate close to this composition is present at Bald Knob. Single-crystal Weissenberg X-ray photographs were obtained from two samples close to the kuthahorite composition to determine if ordering reflections could be observed. The results showed no reflections of the type $h0l$, $l = 2n + 1$, indicating that the space group is $R\bar{3}c$, as for calcite, and suggesting no long-range order for Ca and Mn. Unpublished studies cited by Goldsmith and Graf (1960) indicate that disordering in the compound $CaMn(CO_3)_2$ begins at approximately 450°C. Thus material having the kutnahorite composition should be disordered at temperatures of 550°C, the minimum temperature indicated by the composition of the Bald Knob carbonates. Nevertheless it is surprising that these carbonates close to kutnahorite composition did not attain long-range order upon cooling, despite the relatively long cooling times following regional metamorphism.

Table 2. Analyses of Bald Knob carbonates in weight percent oxide component and mole percent carbonate end member

Sample BK-	weight % MnO	CaO	MgO	FeO	*CO_2	Mol % $MnCO_3$	$CaCO_3$	$MgCO_3$	$FeCO_3$
4-1	32.13	23.11	1.53	1.13	40.42	49.29	44.85	4.14	1.71
4-2	34.81	20.33	1.47	1.25	39.91	54.09	39.97	4.03	1.92
4-4	27.08	18.99	1.27	0.57	39.63	58.03	37.59	3.50	0.88
4-7	31.10	23.62	1.77	0.78	40.22	47.95	46.06	4.81	1.18
4-10	43.71	12.57	1.77	0.87	39.42	68.74	25.01	4.89	1.35
4-12	39.77	16.53	1.71	0.76	39.62	62.24	32.72	3.87	1.18
6-1	39.25	17.67	0.57	0.22	38.97	62.48	35.58	1.60	0.35
6-2	37.99	18.89	0.57	0.18	39.12	60.25	37.89	1.58	0.29
6-3	41.88	15.17	0.58	0.24	38.66	67.21	30.79	1.62	0.39
6-4	44.40	13.21	0.67	0.32	38.83	70.94	26.70	1.87	0.51
8-2	22.56	31.48	0.88	2.08	40.92	24.19	60.36	2.34	3.11
8-6	55.45	3.57	0.61	1.21	38.57	89.10	7.26	1.72	1.91
8-7	56.61	3.26	0.34	0.72	38.45	91.25	6.65	0.95	1.15
8-12	54.96	3.41	0.78	2.51	39.12	87.06	6.82	2.19	3.93
8-18	32.02	20.74	1.85	4.40	40.84	48.61	39.84	4.95	6.60
8-19	27.28	27.10	1.06	2.47	40.85	41.41	52.05	2.84	3.70
10-2	24.84	26.58	1.59	2.52	39.55	38.96	52.75	4.39	3.90
13-1	29.53	16.49	0.53	0.24	38.18	64.21	33.89	1.52	0.38
13-2	39.73	16.60	0.55	0.21	38.41	64.17	33.92	1.58	0.84
14-1	31.66	24.75	0.43	0.24	39.66	49.50	48.96	1.17	0.36
14-2	32.18	24.67	0.41	0.24	39.91	50.01	48.49	1.13	0.36
14-3	31.98	24.70	0.39	0.25	39.79	49.84	48.70	1.07	0.39
14-4	32.16	24.54	0.38	0.23	39.75	50.17	48.42	1.05	0.36
14-5	31.93	24.74	0.42	0.22	39.80	49.75	48.76	1.15	0.34
14-6	31.98	25.11	0.38	0.24	40.09	49.46	49.14	1.04	0.37
17-3	14.00	38.76	1.36	1.50	41.50	20.93	73.29	3.56	2.22
17-4	15.74	37.43	1.14	1.55	41.32	23.62	71.08	3.00	2.29
17-6	14.22	38.71	1.29	1.56	41.55	21.22	73.09	3.38	2.30
17-7	15.09	37.82	1.18	1.60	41.30	22.66	71.86	3.11	2.37
17-10	15.55	37.61	1.11	1.64	41.37	32.31	71.34	2.92	2.43
17-12	15.01	37.66	1.24	1.71	41.26	22.56	71.62	3.28	2.53
17-20	15.22	37.64	1.18	1.41	41.13	22.96	71.82	3.13	2.09
17-21	15.19	37.94	1.28	1.85	41.73	22.58	71.34	3.35	2.72
18-1	27.00	27.16	1.50	1.37	40.53	41.31	52.58	4.04	2.07
18-1-A	26.10	28.83	1.64	1.67	41.62	38.89	54.35	4.30	2.46
18-2	43.15	14.35	1.44	1.39	40.42	66.18	27.83	3.88	2.11
18-2-A	24.40	28.87	1.78	2.08	41.00	36.91	55.25	4.74	3.11
18-3	24.86	29.23	1.52	1.71	41.05	37.56	55.86	4.03	2.54
18-4	25.19	29.56	1.61	1.90	41.74	37.43	55.56	4.21	2.79
18-4-A	24.80	29.04	1.65	1.74	41.03	37.49	55.53	4.38	2.60
18-5	24.12	29.78	1.42	1.54	40.81	36.65	57.24	3.80	2.31
18-5-A	25.69	28.65	1.58	1.61	41.12	38.76	54.66	4.20	2.39
18-6	25.43	28.20	1.60	1.73	40.70	38.75	54.36	4.30	2.60
18-7	24.23	30.09	1.43	1.67	41.23	36.46	58.26	3.80	2.48
18-7-A	26.35	27.75	1.71	1.68	41.01	39.85	53.09	4.55	2.51
18-11	24.57	30.26	1.38	1.65	41.50	36.72	57.22	3.63	2.43
18-11-A	29.15	25.62	1.37	1.30	40.47	44.67	49.66	3.70	1.96
18-13	25.78	28.83	1.50	1.77	41.32	38.69	54.73	3.95	2.62
18-15	25.70	28.82	1.57	1.79	41.35	38.54	54.67	4.13	2.65
18-17	24.75	29.71	1.66	1.99	41.69	36.82	55.92	4.34	2.92
22-1	37.66	20.18	0.24	0.29	39.61	58.95	39.95	0.65	0.45
22-2	38.04	20.48	0.22	0.16	39.98	58.99	40.17	0.59	0.24
22-3	32.87	24.30	0.23	0.13	39.78	51.24	47.91	0.64	0.21
22-4	34.72	23.00	0.21	0.16	39.89	53.97	45.22	0.57	0.24
22-5	33.78	23.78	0.22	0.16	39.94	52.44	46.70	0.61	0.24
22-6	33.00	23.43	0.26	0.17	39.78	52.84	46.19	0.70	0.26
22-7	37.72	20.68	0.23	0.00	39.86	58.68	40.70	0.62	0.00
22-8	35.97	21.52	0.28	0.19	39.60	56.32	42.63	0.76	0.29
50-2	25.24	30.22	0.36	0.06	39.81	39.34	59.56	0.99	0.09
635-2-A	44.62	14.22	0.21	0.19	39.16	70.64	28.47	0.59	0.29
635-5	45.67	13.36	0.25	0.18	39.17	72.28	26.74	0.69	0.29
635-5-A	48.60	11.42	0.25	0.18	39.47	76.33	22.70	0.70	0.27
635-6	43.95	14.36	0.24	0.18	38.88	70.08	28.96	0.68	0.28
635-7	48.69	10.48	0.28	0.15	39.08	77.22	21.75	0.79	0.24
635-8	48.39	10.72	0.25	0.18	38.78	77.34	21.67	0.70	0.29
635-9	48.47	10.66	0.27	0.14	38.78	77.47	21.55	0.76	0.22
635-10	46.93	12.18	0.26	0.12	39.00	74.60	24.50	0.72	0.18

*CO_2 calculated from stoichometry.

Table 3. Analyses of Bald Knob rhodonites and pyroxmangites

Sample BK-	8-1	8-3	8-4	8-5	8-9	8-10	8-11	8-14	8-15	8-16	8-17	8-20	17-0
SiO_2	45.05	44.71	44.75	44.55	44.56	44.77	44.99	44.73	45.27	45.36	45.86	45.22	46.36
Al_2O_3	0.06	0.06	0.07	0.06	0.07	0.06	0.07	0.07	0.07	0.05	0.06	0.04	0.06
FeO*	7.18	2.59	2.54	2.65	1.32	2.77	2.71	3.44	3.66	11.61	11.95	9.21	9.77
MnO	41.33	49.14	49.68	49.26	51.49	49.83	49.56	48.83	48.34	37.77	36.42	40.37	37.02
MgO	1.37	0.52	0.50	0.54	0.34	0.50	0.51	0.73	0.79	2.72	2.86	2.19	3.96
CaO	3.60	1.47	1.32	1.35	1.06	1.25	1.60	1.44	1.83	1.36	2.07	1.78	2.77
ZnO	***n.a.	n.a.	n.a.	n.a.	n.a.	n.a.	n.a.	n.a.	n.a.	n.a.	n.a.	n.a.	n.a.
Total	98.59	98.49	98.86	98.41	98.84	99.18	99.44	99.24	99.96	98.87	99.22	98.81	99.94
	**(rh)	(rh)	(rh)	(rh)	(rh)	(rh)	(rh)	(rh)	(rh)	(pm)	(pm)	(pm)	(pm)
						Cations relative to 3 oxygens							
Si	0.98	0.98	0.98	0.98	0.98	0.98	0.98	0.98	0.99	0.99	0.99	0.99	0.98
Al	0.00	0.00	0.00	0.00	0.00	0.00	0.00	0.00	0.00	0.00	0.00	0.00	0.00
Fe*	0.13	0.05	0.05	0.05	0.02	0.05	0.05	0.06	0.07	0.21	0.21	0.17	0.17
Mn	0.76	0.92	0.92	0.92	0.96	0.92	0.91	0.90	0.89	0.69	0.66	0.75	0.65
Mg	0.04	0.02	0.02	0.02	0.01	0.02	0.02	0.02	0.03	0.09	0.09	0.07	0.12
Ca	0.08	0.03	0.03	0.03	0.02	0.03	0.04	0.03	0.04	0.03	0.05	0.04	0.06
Zn	***n.a.	n.a.	n.a.	n.a.	n.a.	n.a.	n.a.	n.a.	n.a.	n.a.	n.a.	n.a.	n.a.
Sample BK-	17-1	17-5	17-8	17-9	18-3	18-5	18-6	18-8	18-9	18-10	18-12	18-14	18-16
SiO_2	46.21	45.39	45.53	45.60	47.85	47.77	47.58	47.41	47.48	47.55	47.56	47.06	47.43
Al_2O_3	0.06	0.04	0.06	0.06	0.05	0.06	0.05	0.07	0.05	0.06	0.07	0.09	0.07
FeO*	10.55	10.23	10.53	10.35	7.46	7.50	6.88	6.69	5.12	6.84	6.78	5.60	8.07
MnO	35.67	36.78	36.49	37.00	40.26	39.79	40.66	41.05	41.50	40.79	40.62	40.94	38.27
MgO	4.31	3.31	3.29	3.17	3.36	3.34	3.15	2.94	1.78	3.07	3.04	2.10	3.61
CaO	2.87	2.78	2.73	2.72	1.84	1.83	2.12	1.84	4.17	1.83	1.89	3.58	1.87
ZnO	***n.a.	n.a.	n.a.	n.a.	0.11	0.00	0.11	0.08	0.07	0.15	0.06	0.13	0.17
Total	99.67	98.53	98.63	98.90	100.93	100.29	100.55	100.08	100.17	100.29	100.02	99.50	99.49
	**(pm)	(pm)	(pm)	(pm)	(pm)	(pm)	(pm)	(pm)	(rh)	(pm)	(pm)	(rh)	(pm)
						Cations relative to 3 oxygens							
Si	0.98	0.98	0.99	0.99	1.00	1.01	1.00	1.01	1.01	1.01	1.01	1.01	1.01
Al	0.00	0.00	0.00	0.00	0.00	0.00	0.00	0.00	0.00	0.00	0.00	0.00	0.00
Fe*	0.19	0.18	0.19	0.19	0.13	0.13	0.12	0.12	0.09	0.12	0.12	0.10	0.14
Mn	0.64	0.68	0.67	0.68	0.71	0.71	0.73	0.74	0.75	0.73	0.73	0.74	0.69
Mg	0.14	0.11	0.11	0.10	0.10	0.10	0.10	0.09	0.06	0.10	0.10	0.07	0.11
Ca	0.06	0.06	0.06	0.06	0.04	0.04	0.05	0.04	0.09	0.04	0.04	0.08	0.04
Zn	***n.a.	n.a.	n.a.	n.a.	0.00	0.00	0.00	0.00	0.00	0.00	0.00	0.00	0.00

*All Fe assumed to be Fe^{2+}, **(rh) = rhodonite, (pm) = pyroxmangite, ***n.a. = not analyzed.

Pressure estimate for the Bald Knob deposit

A reasonable estimate of the metamorphic pressure which prevailed during the metamorphism of the Bald Knob rocks can be made by utilizing kyanite and sillimanite occurrences in North Carolina (Stuckey, 1965). Kyanite and sillimanite are found in separate occurrences south and southwest of Alleghany County, and they occur in a trend which, if extended, would pass very near the Bald Knob deposit. Applying the temperature data extracted from the carbonates to the kyanite–sillimanite phase boundary of Holdaway (1971) yields a pressure of 5 kbar, consistent with the metamorphic assemblages found in the enclosing mica schists and amphibolites. Uncertainties in this pressure estimate are estimated at ±1 kbar when errors in the experimental determination of the kyanite–sillimanite curve are combined with uncertainties in our thermometry.

The pyroxenoids

Microprobe analyses of 26 pyroxenoids from 3 samples are given in Table 3 and are plotted on a $MnSiO_3$–$CaSiO_3$–$(Mg,Fe)SiO_3$ ternary diagram in Figure 2. The compositions fall into the fields for pyroxmangite and rhodonite respectively. Single-crystal X-ray study of sample BK-18 confirmed the presence of rhodonite and pyroxmangite in separate grains. Universal-stage optical data on analyzed crystals from samples BK-8, BK-17 and BK-18 fell within two groups, corresponding to rhodonite and pyroxmangite, respectively. Averaged optical data values for the two phases are given in Table 4. Grains with relatively low 2V (40–50°) corresponded in every case to pyroxmangites, and grains with high 2V (60–70°) to rhodonites, and these values allow a rapid distinction between rhodonite and pyroxmangite. Subsequent identification of a particular pyrox-

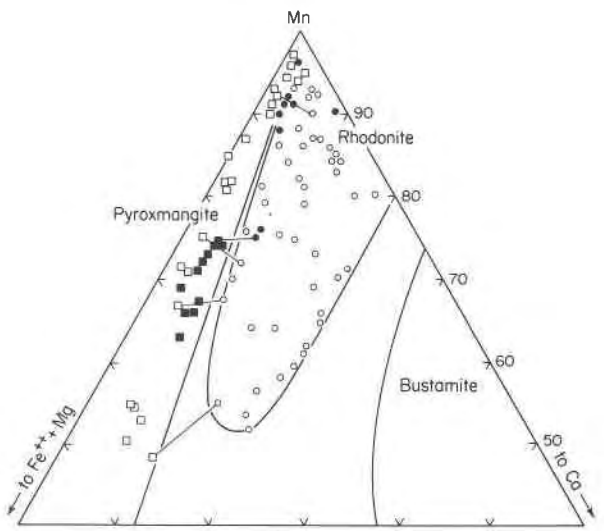

Fig. 2. Compositions of rhodonite (circles) and pyroxmangites (squares). Open circles and squares are data from the literature (Deer *et al.*, 1978; Mason, 1973; Hodgson, 1975; Dickson, 1975; Ohashi and Finger, 1975; Peters *et al.*, 1978; Wall, personal communication, 1978; Tracy *et al.*, 1980; Brown *et al.*, 1980). Solid symbols are from Bald Knob.

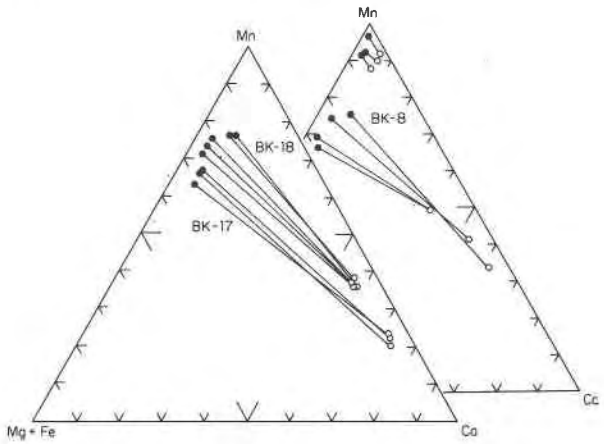

Fig. 3. Compositions of coexisting pyroxenoids (dots) and carbonates (circles). The diagram represents $MnSiO_3$–$CaSiO_3$–$(Mg+Fe)SiO_3$ for the pyroxenoids, and $MnCO_3$–$CaCO_3$–$(Mg+Fe)CO_3$ for the carbonates.

enoid was made by optical measurements and by noting in which field its analysis plotted on the ternary diagram. These fields are well defined by plotting natural rhodonite and pyroxmangite compositions on the ternary diagram (Peacor *et al.*, 1978).

The low Ca content of the pyroxenoids is surprising in view of the high Ca content of coexisting carbonates (Fig. 3). Most of the carbonates coexisting with pyroxenoid contain more than 50 mole % $CaCO_3$ component, and yet the large Ca site in rhodonite is less than 50% filled by Ca. The two Ca sites in pyroxmangite are less than 20% occupied by Ca. Considering that one in five sites for rhodonite (Peacor and Niizeki, 1963) and two in seven for pyroxmangite (Burnham, 1971) prefer to accommodate the large Ca ion, one might expect the carbonate (with over 50% $CaCO_3$ component) to exchange some Ca for some Mn, Mg, or Fe of the coexisting pyroxenoid. However, our data clearly show that the carbonate strongly partitions the Ca over the coexisting rhodonite or pyromangite at Bald Knob *P–T* conditions. Data of Peters *et al.* (1977) show a similar fractionation of Ca between coexisting pyroxenoid and carbonate, and this may be a general effect at moderate grades of metamorphism.

Table 4. Optical data for analyzed pyroxenoid grains from samples BK-8, BK-17, and BK-18

	Rhodonite	Pyroxmangite
$2V_Z$	66°	46°
$c \wedge Z$	40°	40°
$Y \wedge \perp(110)$	50°	30°
$Y \wedge \perp(1\bar{1}0)$	65°	90°

When natural pyroxenoids are found in the system $(Mn,Ca,Mg,Fe)SiO_3$, the coexisting pyroxmangite and rhodonite pairs represent the mutual solubility limits of elements in the two phases, and the width of the miscibility gap will depend on *P–T* conditions, as well as the pyroxenoid compositions. Although a miscibility gap must occur between rhodonite and pyroxmangite (Sundius, 1931; Momoi, 1968; Ohashi *et al.*, 1975; Peacor *et al.*, 1978), few reports of coexisting pairs are available in the literature. Ohashi and Finger (1975) give analyses of pyroxmangite and rhodonite, and Ohashi (personal communication, 1977) informed us that one sample (AK18) contained both phases. Wall (personal communication, 1978) has analyzed two pyroxmangite–rhodonite pairs from Broken Hill, Australia. Peters *et al.* (1978) gave analyses of two pairs from the Alps. Tracy *et al.* (1980) report on a pair from Massachusetts. A number of analyses of coexisting pyroxmangite and rhodonite from Bald Knob are given in Table 3. The pyroxmangite–rhodonite miscibility gap appears to widen somewhat with increasing $(Mg,Fe)SiO_3$. Some overlap may occur between pyroxmangite and rhodonite compositions, presumably due to forma-

tion at different P–T conditions. Higher-temperature rhodonites appear to approach the $MnSiO_3$–$(Mg,Fe)SiO_3$ tieline more closely, overlapping in part with the compositions of more calcic, lower-temperature pyroxmangites. More analyses of pyroxmangite–rhodonite pairs are needed from metamorphic rocks at a variety of P–T conditions to fully explore the relative effects of P and T.

Maresch and Mottana (1976) published a phase diagram for the rhodonite–pyroxmangite transformation in the system $MnSiO_3$, using a combination of their experimental reaction reversals and those of Akimoto and Syono (1972). With reasonable temperature and pressure estimates for the metamorphism of the Bald Knob deposit, we calculated the displacement of the transformation curve due to solid solutions in the pyroxenoids at Bald Knob, in order to test the applicability of the curve for extracting useful pressure data from natural rhodonite–pyroxmangite pairs. The equation of interest is:

$$\Delta G(P_2,T_2) - \Delta G(P_1,T_1) = -\int_{T_1}^{T_2} \Delta S\,dT + \int_{P_1}^{P_2} \Delta V\,dP + RT\ln(K_2/K_1) \qquad (1)$$

Holding T constant and assuming $\Delta V^{\circ}_{298} = \Delta V^{P}_{T}$, equation 1 reduces to:

$$\Delta P = (-RT\ln K)/\Delta V \qquad (2)$$

where $\Delta G = 0$ both at P_1 with $K_1 = 1$ (the experimental equilibrium point in pure $MnSiO_3$ system) and at P_2 (for equilibrium with impure pyroxmangite + rhodonite in the rock). The molar volumes of rhodonite and pyroxmangite were taken from Ito (1972).[4] For the end-member reaction:

$$MnSiO_3 = MnSiO_3$$
$$\text{pyroxmangite} = \text{rhodonite} \qquad (3)$$

the calculated $\Delta V = 0.23 \pm 0.1$ cc and $P_{equil} = 12$ kbar (Maresch and Mottana, 1976). The pressure shift was calculated at 575°C (848 K), but a shift of even ±100°C in the temperature will not materially affect the conclusions. Two quite different activity models were employed in these calculations: the first essentially neglects the partitioning of cations within the two structures in assuming that $a(MnSiO_3) = X(MnSiO_3)$. This model may be realistic if the cations become disordered in the pyroxenoids at high temperature. Some support for this simple model comes from Schwerdtfeger and Muan's (1966) experiments, consistent with ideal mixing of Mn and Fe for the simple system $MnSiO_3$–$FeSiO_3$ at 1150°C. Pressure estimates from this calculation for the Bald Knob rhodonite–pyroxmangite pairs are given in Table 5.

Table 5. Calculated shifts in the rhodonite–pyroxmangite equilibrium

Sample	18-8 Pm	18-9 Rh	18-10 Pm	18-12,14 Rh	18-16 Pm
a_{MnSiO_3}(dis)	.755	.76	.74	.75	.71
ΔP (kb)	-4.1	-8.2	-4.1	-20.9	
P (kb)	+7.9	+3.8	+7.9	-8.9	
X_{Mn} in M_1	.755	.85	.743	.83	.708
M_2	.755	.85	.743	.83	.708
M_3	.755	.85	.743	.83	.708
M_4	.755	.70	.743	.66	.708
M_5	.86	.55	.86	.60	.86
M_6	.51	-	.487	-	.416
M_7	.86	-	.86	-	.86
a_{MnSiO_3}(ord)	.741	.749	.729	.743	.694
ΔP (kb)	-3.5	-8.2	-5.7	-21.0	
P (kb)	+7.9	+3.8	+7.9	-8.9	

The second model considers cation distributions consistent with room-temperature structure refinements in these structures (Peacor and Niizeki, 1963; Burnham, 1971; Ohashi and Finger, 1975; Peacor *et al.*, 1978). For rhodonite all Ca was placed in the M(5) site with Mn alone filling the remaining portion. For M(1)–M(3), Mn and Mg + Fe were partitioned such that Mg + Fe = x where Mg + Fe = $2x$ in M(4) and = 0 in M(5). For pyroxmangite Ca is distributed equally between M(5) and M(7) and the remainder filled with Mn. The sites M(1)–M(4) have Mg + Fe = x where Mg + Fe = $2x$ in M(6) and = 0 in M(5) and M(7). The activity is then calculated site by site and is taken as the product of the mole fraction $MnSiO_3$ on each site. The activity of $MnSiO_3$ in rhodonite is:

$$\alpha^{Rn}_{MnSiO_3}(ord) = (X^{M_1}_{Mn} \cdot X^{M_2}_{Mn} \cdot X^{M_3}_{Mn} \cdot X^{M_4}_{Mn} \cdot X^{M_5}_{Mn})^{1/5} \qquad (4)$$

[4] Narita *et al.* (1977) also obtained unit-cell data on synthetic $MnSiO_3$ rhodonite and pyroxmangite. Calculated unit-cell volumes are 34.93 cc/mole for rhodonite and 34.95 for pyroxmangite, yielding $\Delta V_3 = -0.02$ cc/mole. This ΔV has the wrong sign compared to the experiments, and these data will be ignored below.

and in pyroxmangite is:

$$\alpha^{Pm}_{MnSiO_3}\,(ord) = (X^{M_1}_{Mn} \cdot X^{M_2}_{Mn} \cdot X^{M_3}_{Mn} \cdot X^{M_4}_{Mn} \cdot X^{M_5}_{Mn} \cdot X^{M_6}_{Mn} \cdot X^{M_7}_{Mn})^{1/7} \quad (5)$$

According to this model the activity of $MnSiO_3$ approaches zero as $CaSiO_3$ reaches 1/5 in rhodonite and 2/7 in pyroxmangite, the presumed limits of Ca in these phases. Similarly the activity of $MnSiO_3$ approaches zero as $(Mg,Fe)SiO_3$ goes to 1/2 in rhodonite and 3/7 in pyroxmangite. While these estimates cannot be expected to be exact since activity coefficients have been ignored and because cation distributions are unknown in pyroxenoids at high temperatures, they may be more realistic than assuming random distribution of Mn on all sites as in the first model. The ordered model reduces to the simpler disordered model for random distribution and ideal behavior of Mn on each pyroxenoid site. It attempts to take into account the nonrandom distribution of Mn among the various octahedral sites but must consider ideal mixing on each site because of lack of more complete mixing data.

For the Bald Knob pyroxmangite–rhodonite pairs the two thermodynamic models yield similar pressure estimates of +8 to −9 kbar. Even small analytical errors cause a large shift in estimated pressures. In addition, even small deviations from ideality severely affect the pressures derived—for instance an activity coefficient of 1.1 instead of 1 for one phase will change the pressure shift by some 30 kbar. Even the ±0.1 cc error in the ΔV will cause a 50% change in ΔP. These are effects expected for any reaction with a small ΔV(<1cc), and it is unlikely that this reaction will ever be useful for barometry. As Maresch and Mottana caution, the application of their curve to natural rhodonite–pyroxmangite pairs is premature until the influence of Ca, Mg, and Fe on the relative stabilities of rhodonite and pyroxmangite is better understood.

T–X equilibria and fluid composition

The equilibrium curve for the reaction:

$$MnCO_3 + SiO_2 = MnSiO_3 + CO_2 \quad (6)$$

was determined at 2 kbar and variable H_2O–CO_2 ratios by Peters (1971). Wall and Essene, (1972) calculated it at various pressures from the starting point, using the program EQUILI. Solid solutions in the Bald Knob carbonates and pyroxenoids generally shift these curves to higher temperatures. A knowledge of the temperature and pressure during the metamorphism of the deposit allows an estimation of $X(H_2O)$ and $X(CO_2)$. Peters' (1971) curve for reaction 6 at 2 kbar is shown in Figure 4 compared with the calculated curve. A large discrepancy is noted in the slopes of the experimental *vs.* the calculated curves. The EQUILI computer runs were generated using thermodynamic data for rhodonite, since data for pyroxmangite were lacking. However, applying the relation

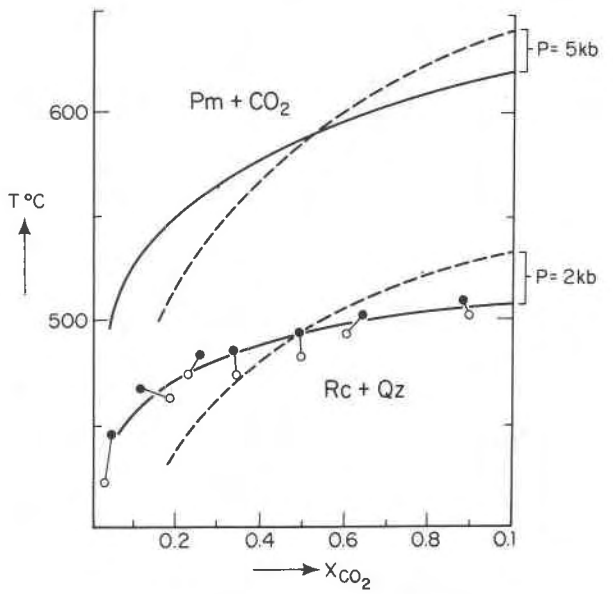

Fig. 4. Peters' curve at 2 kbar for the reaction $MnCO_3 + SiO_2 = MnSiO_3 + CO_2$ compared with the calculated curve using the program EQUILI (Wall and Essene, 1972) from an equilibrium point at T = 494°C and $X(CO_2)$ = 0.55. The solid line is Peters' curve and the dots and circles represent half reversals. The 5 kbar boundary was calculated.

$$\Delta P/\Delta T = \Delta S_r/\Delta V_r \quad (7)$$

to the rhodonite–pyroxmangite transformation curve of Maresch and Mottana (1976) gives a small ΔS_r = +0.28 cal/mol°K for reaction 3. This correction results in a shift of less than 2° for reaction 6 toward lower temperature (assuming ΔV is constant over the P and T range of interest). If one assumes $\Delta S^P_T = \Delta S^\circ_T$, then ΔS is 23.87 cal/mol°K at 500°C for reaction 6. Applying the entropy correction (+0.28 cal/mol°K) and writing reaction 6 for pyroxmangite gives $\Delta S_{reaction}$ = 23.59 cal/mol°K. Inserting this value of ΔS_r into the equation for the slope in T–X space (Kerrick, 1974):

$$dT/dX = RT/\Delta S_r[X(CO_2)] \quad (8)$$

gives a slope consistent with the curve calculated us-

ing EQUILI. However, Peters' curve has a T/X slope of approximately 18°/0.625 at $X(CO_2) = 1.0$, which yields a ΔS_r of about 54 cal/mol°K, implying the unreasonable entropy difference between rhodonite and pyroxmangite of 79 cal/mol°K. This discrepancy could not be resolved, and there appear to be serious errors in Peters' experimental data or in assumptions of mixing of H_2O and CO_2. The following procedure was used to estimate $X(H_2O)$ for the deposit, assuming that Peters' location of the equilibria is approximately correct even though the slope of his experiments seems to be wrong.

(1) T-X equilibria for reaction 6 were calculated using the equilibrium point at 494°C and $X(H_2O) = 0.45$ from Peters' data.
(2) The identical temperature shift with pressure was applied to Peters' curve as was observed for the calculated curves.
(3) The curves were corrected for solid solution using equation 1.

At constant P and T, and $X(CO_2) = 1$, equation 1 reduces to:

$$\Delta G_{\text{reaction}} = RT \ln K \qquad (9)$$

Again, K must be modeled from chemical analyses for rhodonite or pyroxmangite in equilibrium with carbonate and quartz:

$$MnCO_3 + SiO_2 = MnSiO_3 + CO_2 \qquad (10)$$

An ionic ideal model is again used to estimate the activity of $MnSiO_3$ in the pyroxenoid and $MnCO_3$ in the carbonate. Given an experimental P-T-$X(H_2O)$ point where $\Delta G_r = 0$, the EQUILI program calculates ΔG_r at all P-T-$X(H_2O)$ within a specified array. Temperature in equation 10 is taken as the temperature at which the reaction curve, at chosen pressure, intersects the vertical axis of the T-X diagram for $X(CO_2) = 1$. The ΔG_r derived from equation 10 is then added to the ΔG_r at that point (=0), and the temperature shift is calculated from the EQUILI output array. The same temperature correction is then applied to the whole reaction curve. Even though the ideal site by site ionic model is only an approximation for the rhodonite–pyroxmangite reaction, it is thought to be reasonable for decarbonation reactions where most of the free energy change is involved in the fluid.

Calculations based on the Bald Knob pyroxenoid + quartz + carbonate assemblages yielded two limiting cases. The assemblage of sample BK-8-4 yields a ΔG_r of 0.04 kcal at 5 kbar, resulting in a negligible temperature shift of the curve (~2°). The assemblage of sample BK-17-5 gives a ΔG_r of ~2 kcal at 5 kbar, resulting in a temperature correction of ~100°C (Fig. 5). A shift of ±1 kbar produces a change of ±30°C in temperature. While the exact $X(H_2O)/X(CO_2)$ obtained depends on the exact P–T conditions and choice of experimental or calculated curves, it is evident that high $X(H_2O)$ may generally be inferred for the Bald Knob assemblage pyroxenoid + carbonate + quartz.

Metamorphism of the carbonate lenses in the Bald Knob deposit was evidently accompanied by water-rich fluids ($X(H_2O) > 0.5$), even though the deposit was initially composed largely of carbonate + quartz. This suggests that through-going water penetrated the deposit during metamorphism. This may have applied during the metamorphism of manganese deposits elsewhere, and can explain the occurrence of pyroxenoids and other manganese silicates which have been reported at relatively low grades of metamorphism (Huebner, 1967; Peters, 1971; Peters *et al.*, 1973; Peters *et al.*, 1978).

Oxygen and sulfur fugacity

Holland (1959, 1965) has shown the usefulness of calculating oxygen fugacity (fO_2) and sulfur fugacity (fS_2) for a variety of ore deposits and metamorphic rocks. Similar calculations have been made for phases in the systems Mn–Ti–Si–O_2–S_2 and Co–Ti–O_2–S_2 to identify the conditions of metamorphism at Bald Knob. Free energy data for the pertinent phases were obtained from several sources and are summarized in Table 6. Many of the data were taken directly from Robie *et al.* (1978). Data for $MnTiO_3$, Mn_2TiO_4, $CoTiO_3$, and Co_2TiO_4 were calculated from data of Evans and Muan (1971) and Brezny and Muan (1969), based on the free energy of formation of these phases from their constituent oxides at higher temperatures combined with oxide and element entropy data. Given the free energy of formation of a phase at one temperature from the constituent oxides, the free energy of formation of the phase from the elements at other temperatures was obtained by integrating the entropy change of the phase from the elements between the two temperatures. Free energies for cobalt sulfides and for MnS_2 were calculated from data of Mills (1974, p. 223–231) and data for $MnSO_4$ were obtained from Mah (1960). Volume data were taken from Robie *et al.* (1978) or calculated from unit-cell data from Strunz (1970) or the ASTM file.

The various equilibria were calculated in fS_2/fO_2 space (Fig. 5), using the equation:

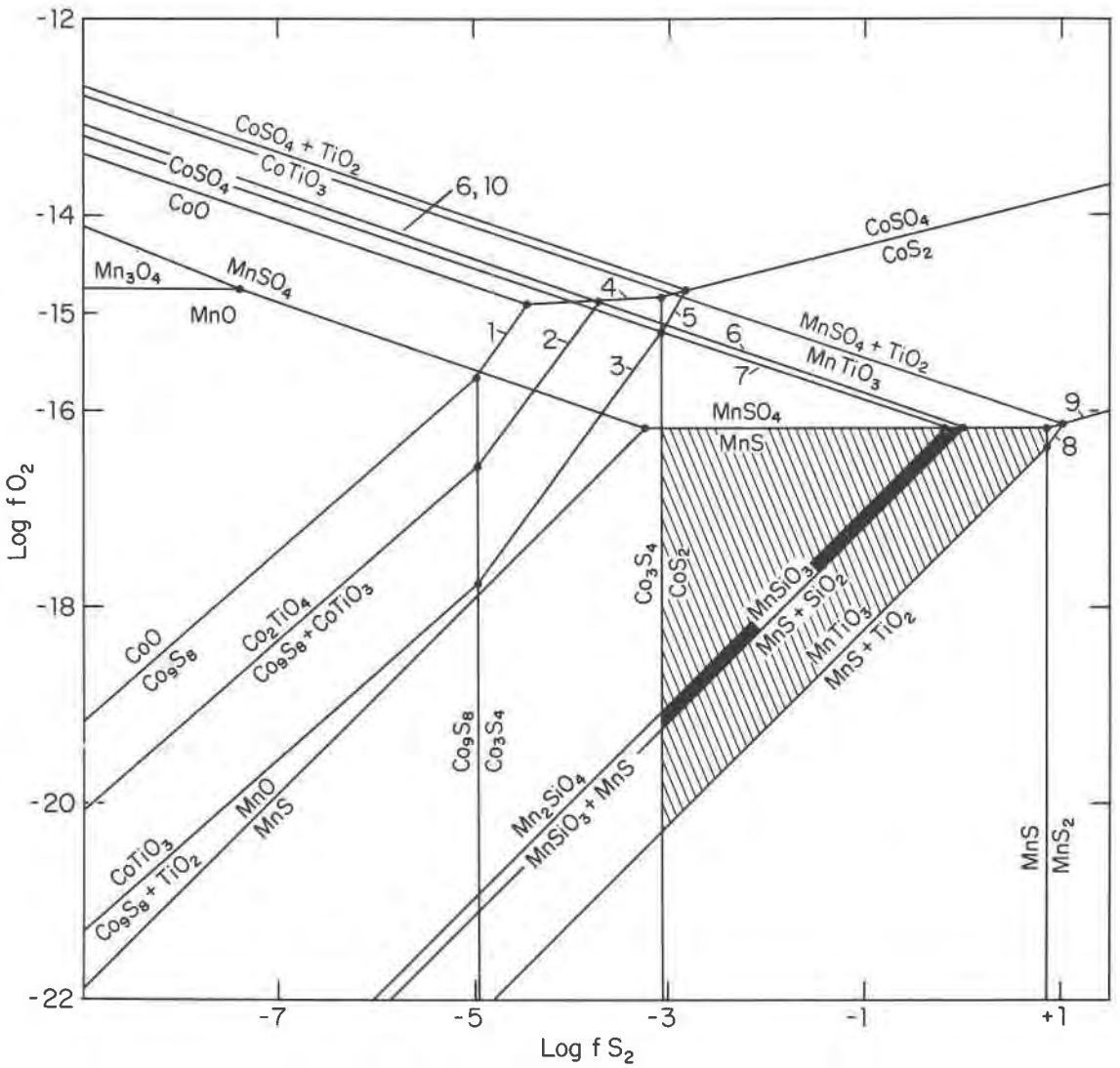

Fig. 5. Log (fO_2)–log (fS_2) phase diagram calculated at 575°C and 5 kbar. The stippled area represents the range of oxygen and sulfur fugacities which prevailed during the metamorphism of the Bald Knob deposit, and the shaded area represents conditions close to those required for pyroxmangite/rhodonite + alabandite + quartz and pyroxmangite/rhodonite + tephroite + alabandite. Reactions 1–10 could not be conveniently labelled on the diagram and are: (1) $6CoO + 4S_2 = 2Co_3S_4 + 3O_2$; (2) $6Co_2TiO_4 + 4S_2 = 2Co_3S_4 + 6\ CoTiO_3 + 3O_2$; (3) $6CoTiO_3 + 4S_2 = 2Co_3S_4 + 6TiO_2 + 3O_2$; (4) $6CoSO_4 + S_2 = 2Co_3S_4 + 12O_2$; (5) $2CoTiO_3 + 2S_2 = 2CoS_2 + 2TiO_2 + O_2$; (6) $2MnSiO_3 + S_2 + 3O_2 = 2MnSO_4 + 2SiO_2$; (7) $2Mn_2SiO_4 + S_2 + 3O_2 = 2MnSO_4 + 2MnSiO_3$; (8) $2MnTiO_3 + 2S_2 = 2MnS_2 + 2TiO_2 + O_2$; (9) $2MnSO_4 + S_2 = 2MnS_2 + 4O_2$; (10) $Co_2TiO_4 + S_2 + 2O_2 = 2CoSO_4 + TiO_2$.

$$\Delta G^{\circ}_{T}(\text{kcal}) = RT\ln[(fO_2)^n/(fS_2)^m] + \Delta V_s\,\Delta P/41.84 + RT\ln K_s \quad (11)$$

where $T = 848°K$ (575°C), $R = 0.001987$ kcal/mol°K, V_s in cc, $\Delta P = 5$ kbar, and n and m are the fluid coefficients as in the following generalized reaction:

$$m \cdot S_2 + X + Y + Z = n \cdot O_2 + A + B + C \quad (12)$$

The equilibrium constant for the solids in equation 11 must be evaluated if there are significant impurities in the solid phases. The standard state is taken to be the pure phase (for the solids) and the ideal gas (for O_2 and S_2) at 1 bar and T. Qualitative data obtained with a solid-state energy-dispersive multichannel analyzer indicate that the sulfide and titanate phases in Bald Knob rocks are more than 90% end-member, and the shift in the oxide–sulfide–sul-

fate equilibria is negligible for solid solutions in these phases at Bald Knob. For rhodonite and tephroite the effect of the solid solutions was again modeled as in Table 6. For example, holding sulfur fugacity constant, the effect of the $RT\ln K_s$ term for an average Bald Knob rhodonite composition is to shift the rhodonite reaction curve in the shaded region of Figure 5 by not more than 0.2 log (fO_2) units. These errors are similar in magnitude to those generated by errors in free energy data. The calculated phase diagram (Fig. 5) is consistent with all observed assemblages at Bald Knob. While it is expressly for 848°K and 5 kbar, the relations will qualitatively apply to other crustal metamorphic manganese deposits. Unfortunately few careful descriptions of accessory titanates and sulfides coexisting with manganese silicates and oxides are available in the literature. One apparent exception to the calculated phase diagram is reported by Peters *et al.* (1977), who record the assemblage alabandite–tephroite–pyroxmangite with hausmannite. Our calculations indicate that hausmannite is incompatible with alabandite and pyroxmangite, but hausmannite may possibly have been confused with jacobsite.

The stability fields of $CoSO_4$ and $MnSO_4$ appear to interrupt reactions of the higher oxides of Co and Mn from the fully sulfidized CoS_2 and the monosulfide MnS. The sulfates are not known in nature, presumably because they are too soluble in aqueous fluids at the relatively high SO_2 pressure they will require. The conditions under which the sulfates are stable may not be reached in Co- and Mn-rich rocks, or if they are obtained may simply cause leaching of Co and Mn from sulfides, silicates, oxides, and titanates, leaving behind materials impoverished in Co and Mn. Indeed, the solution of $CoSO_4$ or $MnSO_4$ in an aqueous fluid may yield values of $a(CoSO_4)$ or $a(MnSO_4)$ considerably reduced from unity, contracting the stability of the oxides and sulfides still further. The high fS_2–fO_2 part of the diagram may then represent the conditions for ore transportation as opposed to the two windows for deposition or stasis at oxidizing and sulfur-poor conditions on the one hand, or reducing sulfur-rich conditions on the other. The highly oxidized manganese deposits involving hausmannite (Mn_3O_4) and other oxidized Mn minerals such as braunite require quite different fO_2/fS_2 conditions than those at Bald Knob.

Table 6. Thermodynamic data used in calculating Fig. 5

Phase	Formula	$-\Delta G^\circ_{848}$(fm) kj/mol·K	ref.	V°_{298} Cc/mol	ref.
cobalt oxide	CoO	172.8	(1)	11.64	(1)
manganosite	MnO	322.8	(1)	13.22	(1)
hausmannite	Mn_3O_4	1,093.3	(1)	46.95	(1)
partridgeite	Mn_2O_3	740.0	(1)	31.37	(1)
pyrolusite	MnO_2	365.4	(1)	16.61	(1)
quartz	SiO_2	757.0	(1)	22.69	(1)
rutile	TiO_2	789.0	(1)	18.82	(1)
cobalt pentlandite	Co_9S_8	778.4	(4)	147.44	(3)
linnaeite	Co_3S_4	320.1	(4)	62.55	(2)
cattierite	CoS_2	125.7	(4)	25.52	(2)
alabandite	MnS	222.5	(1)	21.46	(1)
hauerite	MnS_2	222.0	(4)	34.20	(1)
cobalt sulfate	$CoSO_4$	588.3	(8)	39.94	(3)
manganese sulfate	$MnSO_4$	756.6	(5)	43.62	(1)
cobalt orthotitanate	Co_2TiO_4	1,166.2	(6)	45.38	(2)
cobalt metatitanate	$CoTiO_3$	982.8	(6)	31.05	(2)
pyrophanite	$MnTiO_3$	1,148.7	(7)	32.76	(2)
tephroite	Mn_2SiO_4	1,450.3	(1)	48.61	(1)
rhodonite	$MnSiO_3$	1,104.0	(1)	35.16	(1)

(1) Robie et al. (1978); (2) ASTM; (3) Strunz (1970); (4) Mills (1974); (5) Mah (1960); (6) Brezny and Muan (1969); (7) Evans and Muan (1971); (8) Weller (1965).

Bald Knob fO_2/fS_2 conditions are quite different than those in adjacent rocks and must have been maintained as distinctly different throughout metamorphism. Adjacent amphibolites carry accessory pyrrhotite and magnetite, and require fO_2 several orders of magnitude higher and fS_2 orders of magnitude lower than the manganese deposit at peak metamorphic *P–T*. If a through-going water-rich fluid interacted with the carbonate deposit as concluded above, the fO_2 and fS_2 must have been locally buffered at quite different levels within the manganese deposit. Presumably this condition would have been maintained throughout metamorphism, creating a sulfur-rich and oxygen-poor halo around the manganese deposit as long as the sulfides persisted. To a first approximation it would appear that the Bald Knob protolith was a sulfide- and carbonate-rich body poor in Mn oxides, particularly Mn^{3+} oxides. The consistency of all the phase equilibria supports the contention that it last equilibrated during metamorphism. We have found no evidence inconsistent with a premetamorphic sedimentary origin for the Bald Knob manganese deposit.

Appendix

Microprobe procedure

Element analyses were obtained with an ARL-EMX electron microprobe analyzer with LIF, PET, and TAP wavelength-dispersive crystal spectrometers. An accelerating potential of 15 kV and an emission current of 150 μA were standard operating conditions. A sample current of 0.01 μA was used on Mn silicates and carbonates; the beam current was digitized with

counting times of 20–30 seconds on each of 5–10 areas of each grain analyzed. The presence of minor elements was checked with an energy-dispersive Li-silicon crystal with multichannel analyzer. Spectrometer data were reduced with the Fortran program EMPADR VII written by Rucklidge and Gasparrini (1969).

Carbonates

A natural rhodochrosite from Alma, Colorado, a dolomite from Delight, Maryland, and siderite from Westfalia, Germany were used as standards for all analyses. The compositions of these standards are given in Table 7. Because the specimens were banded, grains from several areas of each sample were analyzed. The data were reduced with the fixed stoichiometry mode with C = Mn + Ca + Mg + Fe (Rucklidge and Gasparrini, 1969).

Pyroxenoids

Synthetic tephroite (provided by Huebner), sphene (provided by Kerrick), and sphalerite (provided by Scott), as well as natural rhodonite (Broken Hill, ANU) and kaersutite (Irving) were used as standards. Analyses of the rhodonite and kaersutite are given in Table 7. Pyroxenoid intergrowths observed on the microscope, as well as discrete grains, were analyzed. Zn and Ti were analyzed for some specimens, and were not found in amounts greater than 0.05 weight percent. Zn and Ti were not included in subsequent analyses.

Table 7. Compositions of standards used for microprobe analyses cited in the text. The synthetic sphene and sphalerite used for the pyroxenoid analyses are stoichiometric

	Alma rhodochrosite	Gabbs dolomite	Westfalia siderite
$MnCO_3$	97.63	0.10	15.77
$MgCO_3$	1.99	46.13	3.78
$FeCO_3$	0.34	0.11	80.01
$CaCO_3$	0.04	53.64	0.44
$ZnCO_3$	0.01	--	0.01
$SrCO_3$	0.02	--	0.01
	Irving kaersutite	**Broken Hill rhodonite**	**Synthetic tephroite**
SiO_2	39.14	45.74	29.75
TiO_2	4.78	--	--
Al_2O_3	14.04	0.07	--
Fe_2O_3	--	1.12	--
FeO	14.40	13.28	--
MnO	0.17	37.80	70.25
MgO	10.68	0.06	--
CaO	10.88	1.31	--
Na_2O	2.80	0.12	--
K_2O	1.56	0.02	--
Cr_2O_3	0.01	--	--

Acknowledgments

We are grateful to J. S. Huebner, D. Burt, and J. Papike for their reviews of the manuscript. We also thank the staff of the electron microprobe laboratory of the University of Michigan, especially L. Allard, for their assistance with the laboratory facilities. We are grateful to J. S. Huebner, D. M. Kerrick, S. D. Scott, and A. J. Irving for providing us with microprobe standards.

References

Akimoto, S. and Syono, Y. (1972) High pressure transformations in $MnSiO_3$. American Mineralogist, 57, 76–84.

Burnham, C. W. (1971) The crystal structure of pyroxferroite from Mare Tranquillitatis. Proceedings, Second Lunar Science Conference, 47–57.

Brezny, B. and Muan, A. (1969) Phase relations and stabilities of compounds in the system $CoO–TiO_2$. Journal of Inorganic and Nuclear Chemistry, 31, 649.

Brown, P. E., Essene, E. J., and Peacor, D. R. (1980) Phase relations inferred from field data for Mn pyroxenes and pyroxenoids. Contributions to Mineralogy and Petrology, in press.

Deer, W. A., Howie, R. A., and Zussman, J. (1978) Rock Forming Minerals, Vol. 2A, Single Chain Silicates. Wiley, New York.

Dickson, B. L. (1975) The iron distribution in rhodonite. American Mineralogist, 60, 98–104.

Evans, L. G. and Muan, A. (1971) Activity–composition relations of solid solutions and stabilities of manganese and nickel titanates at 1250°C as derived from equilibria in the systems $MnO–CoO–TiO_2$ and $MnO–NiO–TiO_2$. Thermochimica Acta, 2, 277–292.

Frondel, C. and Bauer, L. H. (1955) Kutnahorite: a manganese dolomite. American Mineralogist, 40, 748–760.

Goldsmith, J. R. and Graf, D. L. (1957) The system $CaO–MnO–CO_2$: solid solution and decomposition relations. Geochimica et Cosmochimica Acta, 11, 310–334.

Goldsmith, J. R. and Graf, D. L. (1960) Subsolidus relations in the system $CaCO_3–MgCO_3–MnCO_3$. Journal of Geology, 68, 324–335.

Hodgson, C. J. (1975) The geology and geological development of the Broken Hill lode, in the New Broken Hill Consolidated Mine, Australia. Part II, Mineralogy. Journal of the Geological Society of Australia, 22, 33–50.

Holdaway, M. J. (1971) Stability of andalusite and the aluminum silicate phase diagram. American Journal of Science, 271, 97–131.

Holland, H. D. (1959) Some applications of thermochemical data to problems of ore deposits, I. Stability relations among oxides, sulfides, sulfates, and carbonates of ore and gangue minerals. Economic Geology, 54, 184–233.

Holland, H. D. (1965) Some applications of thermochemical data to problems of ore deposits, II. Mineral assemblages and the

composition of ore-forming fluids. Economic Geology, 60, 1101–1129.

Huebner, J. S. (1967) Stability relations of minerals in the system Mn–Si–C–O. Ph.D. Thesis, The Johns Hopkins University, Baltimore, Maryland.

Ito, J. (1972) Rhodonite–pyroxmangite peritectic along the join $MnSiO_3$–$MgSiO_3$ in air. American Mineralogist, 57, 864–876.

Kerrick, D. M. (1974) Review of metamorphic mixed-volatile (H_2O–CO_2) equilibria. American Mineralogist, 59, 729–762.

Mah, A. D. (1960) Thermodynamic properties of manganese and its compounds. U.S. Bureau of Mines Report of Investigations, 5600, 1–34.

Maresch, W. V. and Mottana, A. (1976) The pyroxmangite–rhodonite transformation for the $MnSiO_3$ composition. Contributions to Mineralogy and Petrology, 55, 69–79.

Mason, B. (1973) Manganese silicates from Broken Hill, New South Wales. Journal of the Geological Society of Australia, 20, 397–404.

Mills, K. C. (1974) Thermodynamic Data for Inorganic Sulphides, Selenides and Tellurides. Butterworths, London.

Momoi, H. (1968) Some manganese pyroxenoids. Journal of the Mineralogical Society of Japan, 8, 1–5.

Narita, H., Koto, K. and Morimoto, N. (1977) The crystal structures of $MnSiO_3$ polymorphs (rhodonite- and pyroxmangite-type). Mineralogical Journal, 8, 329–342.

Ohashi, Y. and Finger, L. W. (1975) Pyroxenoids: a comparison of refined structures of rhodonite and pyroxmangite. Carnegie Institution of Washington Year Book, 74, 564–569.

Ohashi, Y., Kato, A., and Matsubara, S. (1975) Pyroxenoids: a variation in chemistry of natural rhodonites and pyroxmangites. Carnegie Institution of Washington Year Book, 74, 561–564.

Peacor, D. R. and Essene, E. J. (1980) Caryopilite—a member of the friedelite rather than the serpentine group. American Mineralogist, 65, 335–339.

Peacor, D. R. and Niizeki, N. (1963) The determination and refinement of the crystal structure of rhodonite, $(Mn,Ca)SiO_3$. Zeitschrift fuer Kristallographie, 119, 98–116.

Peacor, D. R., Essene, E. J., Brown, P. E., and Winter, G. A. (1978) The crystal chemistry and petrogenesis of a magnesian rhodonite. American Mineralogist, 63, 1137–1142.

Peacor, D. R., Essene, E. J., Simmons, Wm. B., Jr., and Bigelow, W. C. (1974) Kellyite, a new Mn–Al member of the serpentine group from Bald Knob, North Carolina, and new data on grovesite. American Mineralogist, 59, 1153–1156.

Peters, Tj. (1971) Pyroxmangite: stability in H_2O–CO_2 mixtures at a total pressure of 2000 bars. Contributions to Mineralogy and Petrology, 32, 267–273.

Peters, Tj., Schwander, H., and Trommsdorff, V. (1973) Assemblages among tephroite, pyroxmangite, rhodochrosite, quartz: experimental data and occurrences in the Rhetic Alps. Contributions to Mineralogy and Petrology, 42, 325–332.

Peters, Tj., Schwander, H., Trommsdorff, V., and Sommerauer, J. (1978) Manganese pyroxenoids and carbonates: critical phase relations in metamorphic assemblages from the Alps. Contributions to Mineralogy and Petrology, 66, 383–388.

Peters, Tj., Valarelli, J. V., Coutinho, J. M. V., Sommerauer, J., and von Raumer, J. (1977) The manganese deposits of Buritirama (Para, Brazil). Schweizerische Mineralogische und Petrographische Mitteilungen, 57, 313–327.

Robie, R. A., Hemingway, B. S., and Fisher, J. R. (1978) Thermodynamic properties of minerals and related substances at 298.15K and 1 bar (10^5 pascals) pressure and at higher temperatures. U.S. Geological Survey Bulletin 1452.

Ross, C. S. and Kerr, P. F. (1932) The manganese minerals of a vein near Bald Knob, North Carolina. American Mineralogist, 17, 1–18.

Rucklidge, J. C. and Gasparrini, E. L. (1969) Specifications of a complete program for processing electron microprobe data: EMPADR VII. Department of Geology, University of Toronto, unpublished circular.

Schwerdtfeger, K. and Muan, A. (1966) Activities in olivine and pyroxenoid solid solution of the system Fe–Mn–Si–O at 1150°C. Transactions of the AIME, 236, 206.

Strunz, H. (1970) Mineralogische Tabellen. 5 Auflage. Akademische Verlagsgesellschaft, Geest und Portig K.-G., Leipzig.

Stuckey, J. L. (1965) North Carolina: Its Geology and Mineral Resources. North Carolina State University Print Shop, Raleigh.

Sundius, N. (1931) On the triclinic manganiferous pyroxenes. American Mineralogist, 16, 411–429 and 488–518.

Tracy, R. J., Lincoln, T. N., Robinson, P., and Ashenden, D. D. (1980) Rhodonite–pyroxmangite–pyroxene–amphibole assemblages. (abstr.) EOS, 61, 390–391.

Wall, V. J. and Essene, E. J. (1972) Subsolidus equilibria in the system CaO–Al_2O_3–SiO_2–H_2O. (abstr.) Geological Society of America Abstracts with Programs, 4, 92.

Weller, W. W. (1965) Low-temperature heat capacities and entropies at 298.15°K of anhydrous sulfates of cobalt, copper, nickel, and zinc. U.S. Bureau of Mines Report of Investigations, 6669, 1–6.

Manuscript received, September 4, 1979;
accepted for publication, July 28, 1980.